

# A NEW VIDEOSONDE FOR IN SITU OBSERVATION OF PRECIPITATION PARTICLES

S. Coquillat, M. P. Boussaton, S. Chauzy, S. Soula, and F. Gangneron

Laboratoire d'Aérodynamique, UMR UPS/CNRS N°5560, Observatoire Midi-Pyrénées, Toulouse, France

**ABSTRACT:** A new balloon-borne instrument for detecting nature, size, and electric charge of precipitating particles in thunderclouds is presented. The sensor is dimensioned to detect the particles singly with sizes ranging from about 0.5 mm to more than 2 cm and charges ranging from  $\pm 1$  pC to  $\pm 400$  pC. The use of a video camera allows to detect the nature of hydrometeors and to observe uncharged particles. Several parameters are deduced from the data processing that involves the probability of detection, which is function of the velocity of four types of particles (raindrops, graupels, aggregates, and hail). An intercomparison experiment between the videosonde and a disdrometer has been carried out with artificial rain at the ground. The measured precipitation rates differ only by 2 % and the size distributions perfectly match for drops with diameter larger than 2.1 mm.

## INTRODUCTION

Several questions on discharge triggering and electrification processes in thunderclouds remain open at the present time. We still don't know which particles, with which electric charge, in which intense electric field, in which volume of intense electric field, are responsible for cloud discharges (11th ICAE, 1999). Blyth et al. (1998) showed that glancing collisions involving at least one raindrop can produce long liquid filaments at the tips of which corona - first step to a propagative discharge - is easily emitted in electric fields down to 150 kV/m. Furthermore, numerical results by Georgis et al. (1995) and others indicate that corona could also be triggered at realistic altitudes from stable raindrops provided their electric charge is high or they interact with another drop. On the other hand, an alternative mechanism based on the acceleration of high energy electrons produced by cosmic rays could lead to propagative discharges too (see Solomon et al., 2001). Further in situ observations of the microphysics involved in the high flash rate events are required for evaluating the probability of occurrence of these various mechanisms.

Microphysics observations can be performed via aircraft measurements using the photodetector shadowing technology (Weinheimer et al., 1991). The simultaneous detection of the electric charge with an induction ring, or even with several electrodes (Murray et al., 1999), is not fully satisfactory since the charge detected does not systematically correspond to the imaged particle. Bateman et al. (1994) designed a balloon-borne sensor that uses optics for determining the particle size. It allows to detect uncharged particles but it cannot provide their nature and shape. However, this information is of importance for determining the in-cloud electrification processes and the relationships between microphysics and lightning activity. Particle nature and shape can be obtained by a cloud particle camera (see Dye et al., 1983) or by a video camera like that used by Murakami and Matsuo (1990) or Takahashi (1990). If the sensor of the formers cannot detect the electric charge of each particle, the special radiosonde of the latter seems the most appropriate sensor for balloon-borne microphysics observation though the viewing volume appears rather small.

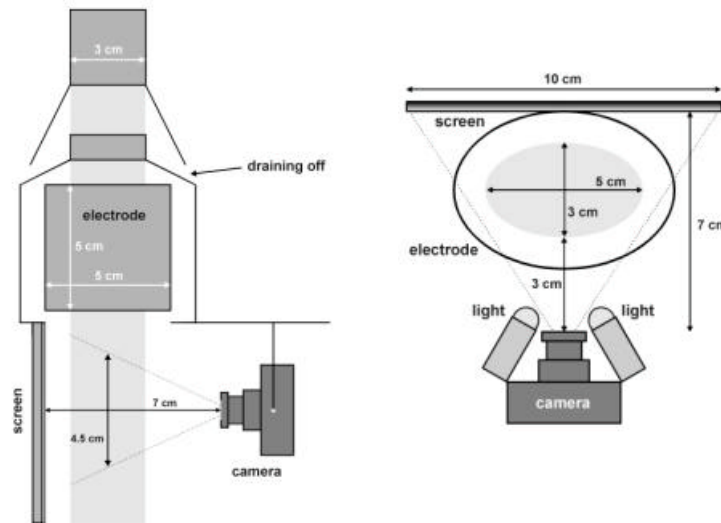
With the aim to investigate the possible relationship between microphysics and lightning flash rate, we plan to perform in-cloud soundings with free balloons carrying a new videosonde. This microphysics sensor will be associated with a meteorological radiosonde and an electric field sensor. Owing to the use of simple technology, we designed a cheap sensor (lost after sounding) that detects the nature, the size, and the electric charge of precipitating particles. Its technical characteristics and performances are described hereafter. The data processing involves the determination of various parameters that are also of importance for the comparison with radar and model data. We present an evaluation of the dimensional distribution  $N(D)$ , the precipitation rate  $R$ , the charge density  $\rho$ , and the radar reflectivity factor  $Z$ . The precipitation rate calculation has been tested at the ground from the comparison between data from the videosonde and from a disdrometer. Further calibration of the charge density determination is currently carried out.

## DESCRIPTION OF THE VIDEOSONDE

As displayed in Figure 1 (left), the videosonde is constituted of several stages. The top inlet has an elliptic section (3 cm  $\times$  5 cm). A second elliptic inlet, 2 cm below, allows to select the particles which trajectory is not too tilted. The rejected particles are drained off by specific openings. Afterwards, the selected particles cross the electrode (elliptic section 5 cm  $\times$  7 cm, 5 cm in height) designed for detecting their electric charge, and pass in front of a CCD video camera. The camera field of view has an angle of about 50° in the vertical plane, and 68° in the horizontal plane. The dimensions of the viewing volume are the result of a balance between a short distance from the camera lens (3 cm) and a large view depth (3 cm). In the direction perpendicular to the optic axis, we increased the inlet dimension up to 5 cm in order to increase the observable volume (Figure 1, right). This is why the sensor section is elliptic. The viewing volume is therefore about 53 cm<sup>3</sup> for an average height of 4,5 cm. It is markedly greater than that - 8.7 cm<sup>3</sup> - of the videosonde by Takahashi (1990), consequently the size

spectrum of observable particles is shifted towards larger sizes. Considering the induction cylinder and the viewing volume, less than one particle (actually 0.35) can be present at each time in the sensor with a 100 mm/h rain rate (see Bateman et al., 1990).

Figure 1: Sketch of the videosonde in the vertical (left) and horizontal (right) planes.



The video camera (12 V, 120 mA) continuously films at a rate of 25 images per second. The deinterlacement of the pictures in the subsequent data processing allows to reach 50 images per second. The aperture time of the camera is automatically set up in function of the existing lighting. Therefore, we used two halogen lights (12 V, 420 mA) to reduce this time in order to get sharp pictures for the largest particles that have the highest fall velocities, taking into account the rate of ascent of the balloon (5 m/s). For maximizing the lighting and avoiding any image saturation by undesirable reflection, the back screen is covered by white diffusing plastic finely sandpapered. We gave up the use of an optical barrier for triggering the camera because the system would have been much more expensive. Moreover, the triggering system of this low cost camera is inaccessible and the response time after each camera start (40 ms) is too large compared to the transit time of the particles in the sensor (about 10 ms). The use of two lights located just beside the camera (see Figure 1) allows retrieving the distance between the observed particle and the camera objective via the location of the induced shadows. This distance is of prime importance for determining the dimensions of the particle (see next section).

The electric charge measurement is driven by the electronics that amplifies, integrates, and filters the electric current induced on the electrode during the passage of a particle. The charge value is digitized when the charge signal rises its maximum amplitude. It is converted in binary code and further displayed with the charge polarity by an array of LED located in the back screen in the field of view of the camera. This display is released during the time the particle is visible from the camera. The detected charge may range from  $\pm 1$  pC to  $\pm 400$  pC. According to Weinheimer (1988), the electric charge can be overestimated if the particle trajectory approaches the induction electrode. We estimated this overestimation in function of the sensor geometry: it may reach a maximum of 8.2 % along the optic axis and a maximum of 25 % in the perpendicular direction. These errors, specific to this kind of charge sensor, cannot be corrected since we are not able to know the particle position inside the induction electrode. The rather large error in the perpendicular direction results from the enhanced viewing volume, which allows on contrary to get more reliable information on particle densities.

The video signal that contains all the information is transmitted to ground by telemetry in real time via a video transmitter (100 mA), about 500 kHz in bandwidth and 30 km in range. The ground receiving antenna is of YAGI type with a 6 m span and a  $2 \times 11^\circ$  aperture angle at  $-3$ dB. The whole electrical consumption of the videosonde rises about 1060 mA. The power supply, regulated only for the camera in order to avoid any surge of voltage at the start, is ensured by 1.5 V lithium batteries which capacity is 2570 mA and weight is low. Electronics and batteries are embedded in a styrofoam case recovered by a thin plastic film for water-proofing and by an aluminium film for shielding. The total mass of the videosonde with its transmitter is about 950 g.

#### DETERMINATION OF THE PARTICLE SIZE

A video picture saved in bitmap format (see Figure 2, left) provides only the apparent size of the observed particle. On one hand, the camera objective induces an optical aberration that needs correction, on the other hand, the closer the particle to the objective, the larger this particle appears, which means that the evaluation of the distance between the particle and the objective is required for determining its real size. Basically, each point in the image is identified by its polar coordinates ( $r, \varphi$ ) in pixels, the origin being at the center of the picture. The distance between two points is calculated after having converted the apparent radius in pixel into the real radius in meter.

The first step consists in correcting the distortion due to the optical aberration, which is purely radial. If we observe a target composed of equidistant concentric circles and located at a distance  $L$  from the camera, the circles are not distorted but the radial distances are modified since the circles far from the center appear closer and closer from each other. To account for this distortion, we performed a 3<sup>rd</sup> order polynomial adjustment between the apparent radius and the real radius. This adjustment was made for reference distances  $L$  varying from 3 cm to 7 cm (back screen) every 0.5 cm.

The subsequent step is to find which polynomial correction is to be used for the observed particle. For that, one needs to know the distance  $\ell$  between the particle and the camera (Figure 2, right). Actually, it is calculated according to the following equation:  $\ell = L d_\ell / (d_\ell + d_0)$ , where  $L = 7$  cm is the maximum distance, i. e. between the camera and the back screen,  $d_\ell$  is the distance between the filaments of both halogen lights, and  $d_0$  is the real distance between the center of both particle shadows on the back screen (see Figure 2). Of course, the real distance  $d_0$  is deduced from the apparent distance between shadow centers corrected with the polynomial adjustment corresponding to  $L = 7$  cm. When  $\ell$  is known, the correction on the apparent size of the particle is a linear interpolation between the corrections corresponding to the reference distances that surround  $\ell$ .

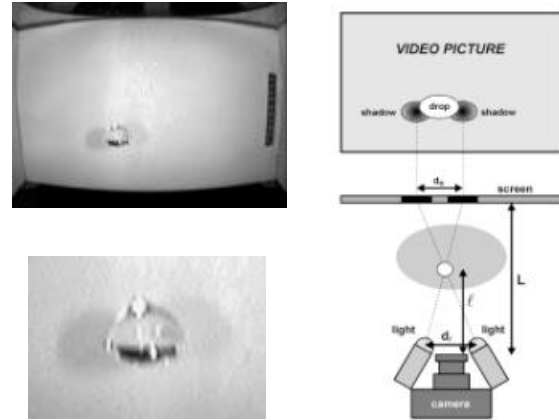


Figure 2: Picture (top left) and corresponding zoom (bottom left) of a large raindrop. Right: sketch of the determination of the distance  $\ell$  between the observed drop and the camera based on the localization of the drop shadows.

This procedure allows to determine the size of the precipitation particles within a 3% average accuracy depending on their location in the camera field of view. The accuracy has been theoretically calculated and experimentally verified by filming a ball of known dimension in a large variety of locations in the viewing volume.

#### ACHIEVABLE PARAMETERS

The determination of several parameters is based on statistical considerations. Given the video sampling period  $T = 20$  ms (50 images per second) and the time  $t = h / V(D)$  during which a particle of diameter  $D$  falls with the velocity  $V(D)$  in the field of view of the camera of average height  $h = 4.5$  cm (see Figure 1), the probability with which the particle can be observed is  $P(D) = 1$  if  $t > T$  and  $P(D) = t / T$  if  $t < T$ . This probability requires thus the knowledge of the velocity, which is calculated for only 4 categories of particles for simplicity (raindrops, graupels, aggregates, and hail) according to the various methods available in the literature. The velocity calculation is also needed for the determination of the sampling volume. The first parameter that can be determined is the size distribution  $N(D)$  for each category of particles. It is given by:

$$N(D) = \frac{n(D)}{P(D) \Delta t A (V(D) + V_{bal}) \Delta D}$$

where  $n(D)$  is the number of particles of diameter  $D$  observed during the time  $\Delta t$ ,  $A$  the cross-sectional area of the sensor,  $V_{bal}$  the ascent velocity of the balloon, and  $\Delta D$  the bin size. Another parameter that can be determined is the charge density  $\rho$ . Its calculation is the same as that presented by MacGorman and Rust (1998), except that each term of the sum is divided by the detection probability which is here averaged because there is no size-charge relationship. Finally, the radar reflectivity factor  $Z$  is calculated in function of the radar wavelength, the dielectric factor, and the radar reflectivity. The latter is computed in function of the sampling volume and of the backscattering cross-sectional area, which is calculated according to Rayleigh and Mie theories in function of the particle size. At last, the precipitation rate  $R$  and the current density  $J$  can be deduced from the size distribution  $N(D)$  and from the charge density  $\rho$ , respectively. All these parameters have a twofold interest, they possess a higher physical sense than individual observations, and they are directly comparable to radar data and model outputs.

#### CALIBRATION

The precipitation rate calculation has been tested at the ground by comparing data from the videosonde and from a disdrometer. Both sensors were submitted during 8 minutes to an artificial shower produced by a lawn sprinkler located 17 meters above in order to ensure all the drops to reach their terminal velocity. The measured

precipitation rates are very similar:  $R = 153.2$  mm/h measured by the disdrometer, and  $R = 155.8$  mm/h (+ 1.7 %) deduced from videosonde observations. The detailed  $N(D)$  distributions are displayed in Figure 3. Both distributions are in very good agreement for drops with diameter larger than 2.1 mm - the last bin in disdrometer data is an accumulation of the largest out of range drop sizes. On contrary, the small drops appear underestimated by the videosonde. The reason is that the somewhat high precipitation rate combined with the black plastic wrapper fixed at the bottom of the videosonde for avoiding undesirable sunlight provoked a splashing that renders pictures difficult to analyze in the case of small drops. One can also point out a difference around 2 mm. This discrepancy probably arises from the electronics of the disdrometer. It has been shown that irregularities in transfer function of the electronics used for diameter classification lead to secondary peaks which can be considered as artifacts (Sheppard, 1995; Sauvageot and Lacaux, 1995). Therefore, the peak around 2.1 mm in the disdrometer data could have appeared at the expense of surrounding diameter classes.

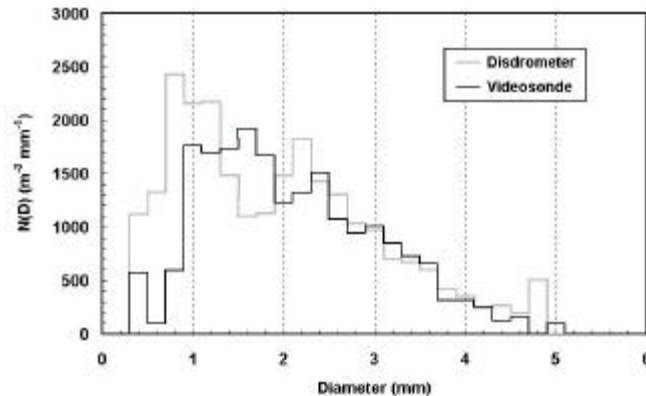


Figure 3: Data comparison between a Joss-Waldvogel disdrometer and the videosonde during a 8 minutes artificial shower.

## CONCLUSION

The new videosonde that will be launched in forthcoming thunderstorms during spring and summer 2003 presents the main advantage to allow the simultaneous detection of the nature, the size, and the electric charge of precipitation particles. The sizes that can be measured range from about 0.5 mm to more than 2 cm in diameter, with an average accuracy of 3 %. The detectable charges range from  $\pm 1$  pC to  $\pm 400$  pC. The relatively large sampling volume of the sensor allows to get more reliable information on cloud microphysics. It induces though a possible overestimation of the electric charge with a maximum amount between 8 and 25 % according to the particle trajectory inside the induction electrode. By taking into account the probability for a particle to be detected – the video sampling rate is 50 images per second – the data processing provides several parameters that are directly comparable to radar data and model outputs.

## REFERENCES

- Bateman, M. G., W. D. Rust, and T. C. Marshall, A balloon-borne instrument for measuring the charge and size of precipitation particles inside thunderstorms, *J. Atmos. Oceanic Tech.*, 11, 161-169, 1994.
- Blyth, A. M., H. J. Christian, and J. Latham, Corona emission thresholds for three types of hydrometeor interaction in thunderclouds, *J. Geophys. Res.*, 103, 13975-13977, 1998.
- Dye, J. E., B. E. Martner, and L. J. Miller, Dynamical-microphysical evolution of a convective storm in a weakly-sheared environment. Part I: Microphysical observations and interpretation, *J. Atmos. Sci.*, 40, 2083-2096, 1983.
- Georgis, J. F., S. Chauzy, and S. Coquillat, Computed conditions of corona emission from two interacting raindrops, *Q. J. R. Meteorol. Soc.*, 121, 1853-1866, 1995.
- MacGorman, D. R., and W. D. Rust, *The electrical nature of storms*, 422 pp., Oxford University Press, New York, USA, 1998.
- Murakami, M., and T. Matsuo, Development of the hydrometeor videosonde, *J. Atmos. Ocean. Tech.*, 7, 613-620, 1990.
- Murray, W. C., W. P. Winn, R. J. Thoms, A. E. Ebnetner, P. R. Fleischhacker, R. P. Lawson, K. A. Weaver, R. Stewart, and C. Wieland, Aircraft measurements of particule image and charge inside a New Mexico thundercloud, *Proceedings of the 11th Int. Conf. Atmos. Elec.*, Guntersville, USA, 260-263, 1999.
- Sauvageot, H., and J. P. Lacaux, The shape of averaged drop size distributions, *J. Atmos. Sci.*, 52, 1070-1083, 1995.
- Sheppard, B. E., Effect of irregularities in the diameter classification of raindrops by the Joss-Waldvogel disdrometer, *J. Atmos. Oceanic Tech.*, 7, 180-183, 1990.
- Solomon, R., V. Schroeder, and M. B. Baker, Lightning initiation – conventional and runaway – breakdown hypotheses, *Q. J. R. Meteorol. Soc.*, 127, 2683-2704, 2001.
- Takahashi, T., Near absence of lightning in torrential rainfall producing Micronesian thunderstorms, *Geophys. Res. Lett.*, 17, 2381-2384, 1990.
- Weinheimer, A. J., J. E. Dye, D. W. Breed, M. P. Spowart, J. L. Parrish, T. L. Hoglin, and T. C. Marshall, Simultaneous measurements of the charge, size, and shape of hydrometeors in an electrified cloud, *J. Geophys. Res.*, 96, 20809-20829, 1991.
- Weinheimer, A. J., The charge induced on a conducting cylinder by a point charge and its application to the measurement of charge on precipitation, *J. Atmos. Oceanic Tech.*, 5, 298-304, 1988.